Semi-analytical modelling of variable stiffness laminates with discontinuities

Janssens, T.A.; Castro, Saullo G.P.

DOI
10.2514/6.2021-0440

Publication date
2021

Document Version
Final published version

Published in
AIAA Scitech 2021 Forum

AIAA SciTech Forum
11–15 & 19–21 January 2021, VIRTUAL EVENT
AIAA Scitech 2021 Forum

10.2514/6.2021-0440

Semi-Analytical Modelling of Variable Stiffness Laminates with Discontinuities

Thomas A. Janssens* and Saullo G. P. Castro†
Delft University of Technology, Kluyverweg 1 2629HS Delft

Designs taking advantage of fibre-steered laminated manufacturing can optimally vary the stiffness and strength properties of high-performance structural components according to the geometry, loads and boundary conditions. For the stability behaviour of laminates with discontinuities such as local reinforcements and cut-outs, variable stiffness laminates have the additional ability to decrease stress concentration factors, increase buckling loads and decrease the negative effects of a cut-out; outperforming traditional straight-fibre designs. With the aim of finding closed-form analysis methods or methods with a reduced computational cost, the present study proposes a semi-analytical framework to analyze the stability behaviour of variable stiffness laminates with local reinforcements and cut-outs. Due to the discontinuous nature of the displacement field in these structures, the approximation functions are enriched to capture the behaviour near the discontinuity. In order to determine the energy functional derivatives across the laminate domain, Gauss-Legendre Quadrature numerical integration rules are applied to both rectangular and circular domains and the resultant energies are obtained by subtracting the integration of the cut-out domain from the full domain. A displacement-based formulation is used for the out-of-plane field variable, whereas a stress-based approach is used for the in-plane pre-buckling stress state. The model is set-up for balanced and symmetric laminates, thus decoupling the out-of-plane and the in-plane behaviours. A thorough verification is performed against existing models in the literature and against finite element results. The results for various plates and laminates with varying discontinuities and variable stiffness properties show a good agreement for both in-plane and out-of-plane field variables, ultimately leading to an accurate prediction of the stability behavior of structures with discontinuities.

I. Introduction

Composite materials have become more widespread across the aerospace industry. The use of fibre reinforced polymers, or composites, allow designers to tailor a design for a specific function and can create structures with high strength/stiffness to weight ratios. Conventional composite laminates are composed of multiple layers, or laminae, in which the fibre direction can be aligned with the directions where strength and stiffness are required. Traditional tailoring is done by varying the direction of the fibres and amount of layers for a laminate. Restricting the design to straight fibres however, limits the potential of the fibre composite materials in cases where the strength and stiffness requirements are not uniform across a laminate. For instance in cases of buckling or when the laminate has a cut-out. With a traditional layup design philosophy, the laminate will contain stiffness and strength even at locations where it might not be needed, i.e. additional unnecessary weight. Varying the fibre orientation within a single ply will allow the designer to use even more of the potential provided by fibre composite materials. This application of Variable Angle Tow (VAT) laminates, also known as variable stiffness laminates, thus broadens the design space, allowing the designer to achieve better designs for a given application. In previous work, [1–3] the improvements of performance for these variable stiffness laminates has been demonstrated. However, when structures include cut-outs, often computationally and license-fee expensive finite element (FE) software is used. When designing for a structure with a cut-out, it is of importance to know the effects of the presence, location and size of the cut-out. For traditional materials, e.g. metals such as aluminium, the effects of cut-outs have been studied for decades and are well understood. Furthermore, while the behaviour for isotropic materials is well understood, the effects for composite materials are dependant on the specific layup used. When considering VAT laminates, with the fibre orientation varying throughout a single layer, the effects become more complicated again. This paper is based on the work by Janssens [4], where a new method of determining the mechanical behaviour for plates with cut-outs is introduced. An analytical model has been set-up using

*Corresponding author. MSc Graduate, Aerospace Structures and Materials, janssens.ta@gmail.com
†Corresponding author. Assistant Professor, Aerospace Structures and Materials, S.G.P.Castro@tudelft.nl

the Rayleigh-Ritz method. However, due to the discontinuity created by the presence of the cut-out, the integration of the structural matrices is not performed analytically, but using the Gauss-Legendre Quadrature, thus arriving at a semi-analytical model. The definitions for the variable stiffness laminates can vary from using discrete stiffness changes to linear variation along a single axis, or even non-linear variation along both the x and y axes. In the work, the discrete stiffness change and linear variation are presented. Due to the discontinuous nature of the laminate, either a cut-out or a sudden change of stiffness, the homogeneous solutions in the Rayleigh-Ritz method can take many terms to converge to a solution. To overcome this, the enriched Rayleigh-Ritz method is used, as proposed by Huang et al. [5] and Milazzo et al. [6], to add additional enriching series of functions to describe the behaviour close to the discontinuity. Each of the 'building blocks' described above are discussed in this paper.

II. Variable stiffness laminates

With variable stiffness laminates, the stiffness parameters across the laminate domain are are dependent on the location along the laminate domain. Therefore, the stiffness matrix relating the in-plane distributed forces and moments with the strains, widely known as **ABD** matrix, become variable across the domain, as represented below:

$$\begin{bmatrix} \mathbf{A} & \mathbf{B} \\ \mathbf{B} & \mathbf{D} \end{bmatrix} = \begin{bmatrix} \mathbf{A}(x,y) & \mathbf{B}(x,y) \\ \mathbf{B}(x,y) & \mathbf{D}(x,y) \end{bmatrix}$$

Variable stiffness is still a rather broad expression, and here three different options will be discussed. **The first** consists of discrete changes in the stiffness, either by locally adding or subtracting a laminae. **The second** is a linear variation of the fibre paths throughout each laminae producing variable stiffness by means of different in-plane stiffnesses terms; and finally **the third option** is a non-linear variation of the fibre path in a laminae. Note that, in the present study, coupled variable thickness due to the presence of overlaps created during tow steering [7, 8], will not be investigated.

A. Local reinforcements

Examples of local stiffness changes are reinforcing the outs edges of a laminate, in order to increase the buckling load, as has been done by Biggers & Srinivasan [9] and Kassapoglou [10], as seen in figure 1.

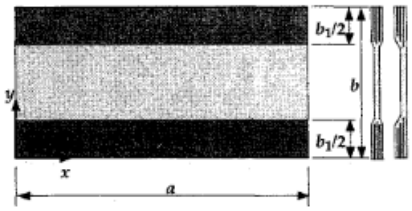

(a) Image from [9]

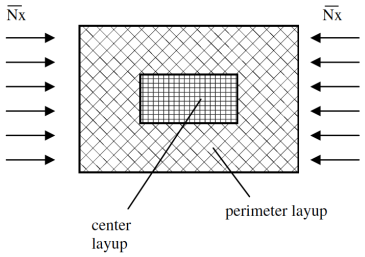

(b) Image from [10]

Fig. 1 Local reinforcements

B. Linear variation of fibre angle

The second option was introduced by Gürdal & Olmedo [1], where the fibre angle is varied along the length of the plate linearly according to the expression in Eq. 1, where a denotes the laminate length. The consequent fibre path with $T_0 = 45$ and $T_1 = 0$ is shown in Fig. 2a.

$$\Phi(x) = \frac{2(T_i - T_0)}{a}x + T_0 \tag{1}$$

C. Non-linear variation of fibre angle

Rather than varying the fibre direction only with respect ot the x direction, a variation can also be determined using a non-linear fibre path definition, such as shown by Wu et al. and Guimaraes et al. [3, 11], described in Eq. 2 where Φ_i

is the ply reference angle and T_{mn} are the control angles in the reference points, as illustrated in Fig. 2b.

$$\theta(x,y) = \Phi_i + \sum_{m=0}^{M-1}\sum_{n=0}^{N-1} T_{mn} \prod_{m\neq i} \frac{x - x_i}{x_m - x_i} \prod_{n\neq j} \frac{y - y_j}{y_n - y_j} \tag{2}$$

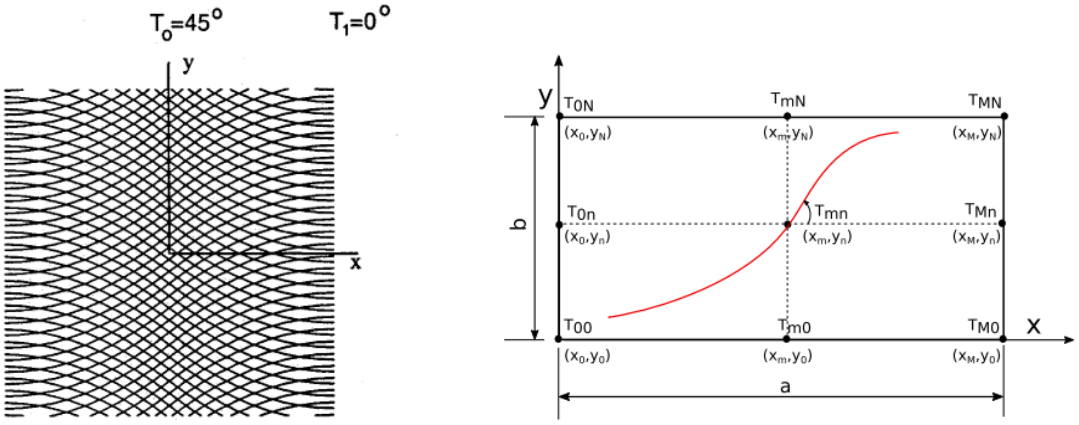

(a) Linear, image from [1]. **(b) Non-linear, image from [11].**

Fig. 2 Fibre paths using linear and non-linear definitions from Eqs. 1 and 2 respectively.

III. Modelling

The model uses the energy method to define the total energy in a body, where the total energy consists of the internal energy, or strain energy U, and the potential energy V. The goal is to find the point where the total energy is at a minimum, i.e. its derivative is equal to zero. For the analysis, both the Total Potential Energy (TPE) and the Total Complementary Energy (TCE) are used. The TPE is used for the out-of-plane behaviour of the laminates where the energy is expressed in terms of the displacements, as shown in Eq. 3 where the laminate domain is denoted by Ω. This work only considers symmetric and balanced laminates, thus the coupling terms ($\mathbf{B}_{ij} = 0$), allowing the de-coupling of the in-plane and out-of-plane analyses.

$$U = \frac{1}{2}\iint_\Omega \begin{Bmatrix} D_{11}\left(\frac{\partial^2 w}{\partial x^2}\right)^2 + 2D_{12}\,\frac{\partial^2 w}{\partial x^2}\frac{\partial^2 w}{\partial y^2} + 4D_{16}\,\frac{\partial^2 w}{\partial x^2}\frac{\partial^2 w}{\partial x \partial y} \\ +D_{22}\left(\frac{\partial^2 w}{\partial y^2}\right)^2 + 4D_{26}\frac{\partial^2 w}{\partial y^2}\frac{\partial^2 w}{\partial x \partial y} + 4D_{66}\left(\frac{\partial^2 w}{\partial x \partial y}\right)^2 \end{Bmatrix} dx\, dy \tag{3}$$

The TCE, where the energy is expressed in terms of stresses, is used for the in-plane behaviour of the laminates. The expressions for the strain energy for the TCE is shown in Eq. 4. The inverse of the **ABD** matrix is denoted by the lower case notation **abd**.

$$U = \frac{1}{2}\iint_\Omega \left(a_{11}N_x^2 + a_{22}N_y^2 + 2a_{12}N_xN_y + a_{66}N_{xy}^2\right) dx\, dy \tag{4}$$

A. Pre-buckling behaviour

In the modelling of the pre-buckling, or in-plane, behaviour, the TCE is used. In this approach approximation functions must be used for the in-plane loads N_x, N_y and N_{xy}. These loads can be reduced to a single unknown function to be approximated using the Airy stress function, shown in Eq. 5. In order to define the approximation functions for Φ, the boundary conditions must be defined. In this work, the laminates are under a uni-axial compressive load. The potential energy thus consist of the axial loads with corresponding deformations, as shown in Fig. 6 where a and b denote the laminate length and width, and u the axial deformation due to the compression.

$$N_x = \frac{\partial^2 \Phi}{\partial y^2} \qquad N_y = \frac{\partial^2 \Phi}{\partial x^2} \qquad N_{xy} = -\frac{\partial^2 \Phi}{\partial x \partial y} \tag{5}$$

$$V = -\int_0^b \left[N_x \cdot u \right]_{x=0}^{x=a} dy \tag{6}$$

This load can be either a uniform compressive force or a uniform compressive displacement, both cases will be examined. When considering an applied displacement u at the outer vertical edges, the load distribution along these edges will be non-uniform due to the variable stiffness, either due to VAT or the presence of a cut-out. This load distribution is unknown and is approximated using an added set of trial functions, Φ_0. According to the boundary conditions, visualised in Fig. 3a, N_{xy0} is zero at the vertical edges. This is not necessarily the case for N_y, but the behaviour for N_y near the edges should follow from the choice of trial functions for the entire domain. So the Φ_0 functions are added only to comply with the edge compressive load N_{x0}. They are thus only related to the edge load N_{x0}, i.e. $\partial \Phi_{0,yy} \neq 0$ and $\Phi_{0,xx} = \Phi_{0,xy} = 0$. As the Φ_0 function only relates to the N_{x0} distribution along the vertical edges, it is only a function of y. Please note, the derivative $\frac{\partial^2 \Phi_0}{\partial y^2}$ is written as $\Phi_{0,yy}$ for legibility.

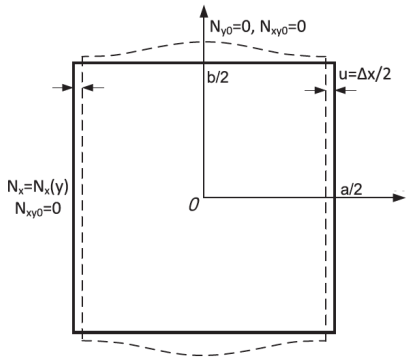

(a) The laminate geometry, uniform compressive loading and boundary conditions. Image from [3].

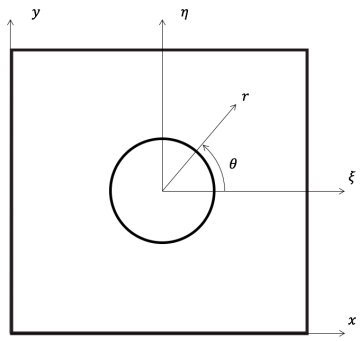

(b) Coordinate systems used in this work.

Fig. 3

In this work, as in the thesis by Janssens [4], four sets of approximation functions are used, as shown in Eq. 7. These sets of functions are defined in various coordinate systems, depending on the type of functions chosen and their suitability. These different coordinate systems can be seen in Fig. 3b, where the natural coordinates, ξ and η range from $[-1, 1]$, x, y range from $[0, a]$, $[0, b]$, θ ranges from $[0, 2\pi]$ and r starts from 0 and is made non-dimensional by dividing with the smaller value of a or b. Functions Φ_0 describe the applied force distribution along the vertical edges of the laminate. Functions Φ_1 describe the behaviour across the entire laminate and combined with Φ_0 is considered as the homogeneous solution, i.e. the solution for a laminate without cut-out in accordance with the work by Wu et al. [3]. Functions Φ_2 and Φ_3 are the enriching functions and are added to describe the behaviour close to the discontinuity.

$$\Phi(x, y) = \Phi_0(y) + \Phi_1(x, y) + \Phi_2(x, y) + \Phi_3(x, y) \tag{7}$$

As the Φ_0 function is used to comply with the N_{x0} distribution at the vertical edges, the Φ_1, Φ_2 and Φ_3 functions should yield a zero N_x at the vertical edges, while N_y is not necessarily zero. For the transverse edges, the opposite is true. As the transverse edge are allowed to deform freely, they are stress free ($N_{y0} = N_{xy0} = 0$), but N_x is not necessarily zero. In the case of a cut-out, the trial functions should account for the stress-free state at the cut-out edges. The normal stress and tangential shear stress with respect to the cut-out edge should yield a zero result. The sets of trial functions must be chosen with these boundary conditions in mind. It was observed by Janssens, that the boundary conditions along a cut-out edge results in complicated conditions when considering multiple coordinate systems [4]. To overcome the problem, a residual thickness is used, whereby the thickness for a cut-out is reduced to 2% of the thickness of the surrounding structure. The value of 2% was chosen by Janssens following a sensitivity analysis [4]. Removing the

complete thickness would yield results that would not comply with the boundary conditions along the edge of the cut-out, as the approximation functions could not enforce this. Rather, leaving a 2% thickness the cut-out region is made sufficiently weak, such that is does not carry any load, but still contains material forcing the model to account for the equilibrium conditions within the laminate.
Due to the approach, the approximation functions Φ_1, Φ_2 and Φ_3 do not take into account the boundary conditions along the cut-out edge.

The approximation functions for Φ_0 and Φ_1 are adopted from the work by Wu et al. and consist of Legendre polynomials as defined in Eq. 8. The Legendre polynomials are chosen because they capture localised behaviour well due to the non-periodic nature of the successive polynomials with respect to trigonometric functions [12–14]. Moreover, with Legendre polynomials the choice between simply-supported, clamped or free boundary conditions is done by simply including or not the first terms in the series [12, 15, 16], in contrast with penalization-based approaches for linear [17–19] and non-linear semi-analytical approaches [20–23]. It has been mentioned that at the vertical edges, the Φ_0 functions only describe the N_{x0} behaviour, i.e. $\Phi_{0,yy}$. Since the functions $\Phi_{0,xx}$ and $\Phi_{0,xy}$ are zero by definition, only the $\Phi_{0,yy}$ functions need to be defined. The series solution is presented in Eq. 9.

$$L_0 = 1, \quad L_1 = \xi, \quad L_2 = \frac{1}{2}(3\xi^2 - 1)$$
$$(n+1) \cdot L_{n+1} = (2n+1) \cdot \xi \cdot L_n - n \cdot L_{n-1} \tag{8}$$

$$N_{x0} = \Phi_{0,_{yy}} = \sum_{k=0}^{K} c_k \cdot \phi_{0,yy} = \sum_{k=0}^{K} c_k \cdot L_k(y) \tag{9}$$

Where L_k are the Legendre polynomials, which are multiplied by unknown coefficients c_k. This definition thus complies with $\Phi_{0,xx}$ and $\Phi_{0,xy}$ being equal to zero. From Eq. 8, the first term in the Legendre series solution is a constant. The case where a uniform force is applied rather than a uniform displacement is thus recovered if only a single term is used for Φ_0 function. The Φ_1 functions are composed of Legendre polynomials also, but now using the (ξ, η) coordinates. To comply with the stress free conditions described previously and shown in Fig. 3a, they are multiplied with a boundary condition forcing function. The Legendre polynomials are multiplied as shown in Eq. 10, and the final expression for Φ_1 is given in Eq. 11.

$$X_i = (1-\xi^2)^2 \cdot L_i(\xi)$$
$$Y_j = (1-\eta^2)^2 \cdot L_j(\eta) \tag{10}$$

$$\Phi_1 = \sum_{i=0}^{I} \sum_{j=0}^{J} A_{ij} \cdot X_i(\xi) \cdot Y_j(\eta) \tag{11}$$

In the work by Janssens [4], a new set of functions is introduced inspired by the work by Huang et al. [5] and Milazzo et al. [6], who simulated the presence of cracks by means of the Ritz method. These functions use the (r, θ) coordinate system and are composed of trigonometric functions. Similar to the functions for Φ_1, the functions are multiplied with a boundary condition function, g_ϕ. The functions are shown in Eqs. 12 and 13.

$$\Phi_2 = g_\phi(\xi, \eta) \cdot \sum_{m=0}^{M} \sum_{n=0}^{N} B_{mn} \cdot cos(m\pi r) \cdot cos(n\theta) \tag{12}$$

$$\Phi_3 = g_\phi(\xi, \eta) \cdot \sum_{m=1}^{M} \sum_{n=1}^{N} C_{mn} \cdot sin(m\pi r) \cdot sin(n\theta) \tag{13}$$

$$g_\phi(\xi, \eta) = (1-\xi^2)^2 \cdot (1-\eta^2)^2$$

With the entries for Φ_0, Φ_1, Φ_2 and Φ_3, the expression in Eq. 7 can be completed. The system can then be minimised with respect to the unknown coefficients A_{ij}, B_{mn}, C_{mn} and c_k, set equal to zero and subsequently solved for the coefficients. The expression for the potential energy however also consists of functions including the unknown c_k. The system to be solved will thus include these coefficients. The system is shown in Eq. 14

$$\begin{bmatrix} \mathbf{K} & \mathbf{K_C} \\ \mathbf{K_C}^T & \mathbf{C} \end{bmatrix} \begin{Bmatrix} \varphi \\ \mathbf{c} \end{Bmatrix} = \begin{Bmatrix} \mathbf{0} \\ \mathbf{Px0} \end{Bmatrix} \tag{14}$$

Where the $\mathbf{K}$ entry is the result from the term $\phi_{i\neq 0} \cdot \phi_{i\neq 0}^T$, the $\mathbf{K_C}$ entry is the result from the terms $\phi_{0,yy} \cdot \phi_{(i\neq 0)}^T$ and the $\mathbf{C}$ entry is the results from the term $\phi_{0,yy} \cdot \phi_{0,yy}^T$. On the RHS the vector $\mathbf{Px0}$ is the result from the $\phi_{0,yy}$ terms in the potential energy Eq. 6. The vector on the LHS contains the coefficients, where φ resembles the coefficients A_{ij}, B_{mn} and C_{mn}, and $\mathbf{c}$ resembles the coefficients c_k.
For the full derivation of these expressions, see Appendix A.

B. Buckling behaviour

To determine the buckling behaviour, the pre-buckling stresses determined in the previous section are used and coupled to a system to determine the out-of-plane behaviour. This system uses the TPE with approximation functions for the deflection w input into Eq. 3. The potential energy is determined using the non-linear mid-plane strains to arrive at the expression in Eq. 15.

$$V = \frac{1}{2} \iint_{\Omega} \left\{ N_x \left(\frac{\partial w}{\partial x}\right)^2 + N_y \left(\frac{\partial w}{\partial y}\right)^2 + 2N_{xy} \left(\frac{\partial w}{\partial x}\right)\left(\frac{\partial w}{\partial y}\right) \right\} dx\, dy \tag{15}$$

The approximation functions for the deflection w are again composed of a homogeneous set and enriching functions. The final expression consists of three sets of functions and is shown in Eq. 16. The expressions for w_1, w_2 and w_3 are shown in Eqs. 17 through 19. Unlike using the TCE with approximation functions for the stresses, there are no geometrical boundary conditions for the laminate at the cut-out edge, thus they are free and no additional conditions need to be met.

$$w = w_1(x,y) + w_2(x,y) + w_3(x,y) \tag{16}$$

$$w_1(x,y) = \sum_{i=1}^{I} \sum_{j=1}^{J} A_{ij}\ sin\left(\frac{i\pi x}{a}\right)\ sin\left(\frac{j\pi y}{b}\right) \tag{17}$$

$$w_2(x,y) = g_w(\xi,\eta) \cdot \left\{ \sum_{m=1}^{M} \sum_{n=0}^{N} B_{mn} \cdot (1-r)^m \cdot cos(n\theta) \right\} \tag{18}$$

$$w_3(x,y) = g_w(\xi,\eta) \cdot \left\{ \sum_{m=1}^{M} \sum_{n=1}^{N} C_{mn} \cdot (1-r)^m \cdot sin(n\theta) \right\} \tag{19}$$

$$g_w(x,y) = (1-\xi^2) \cdot (1-\eta^2)$$

Inputting these expressions into Eq. 16 and subsequently into the expression for U and V in Eqs. 3 and 15 respectively, the eigenvalue problem in Eq. 20 is obtained.

$$[\mathbf{K} + \lambda \mathbf{F}]\ \{c\} = 0 \tag{20}$$

In Eq. 20 the parameter λ denotes the eigenvalues, $\boldsymbol{K}$ is the stiffness matrix resulting from the minimisation of strain energy Eq. 3 and $\boldsymbol{F}$ is the matrix resulting from the minimisation of the potential energy in Eq. 15. The inputs for N_x, N_y and N_{xy} in the potential energy are obtained from the in-plane load distribution. As the eigenvalues λ are in relation to the applied loading, they resemble the applied load used to determine the inputs N_x, N_y and N_{xy} in Eq. 14.

C. Numerical modelling

As mentioned, a Gauss-Legendre Quadrature numerical integration scheme is used for he integration. The integration for the full, rectangular domain is reasonably straightforward and has been documented by many authors and textbooks. The integration for the discontinuity, a square insert, a circular insert or a circular cut-out is less straightforward. The procedure to find the circular integration points and corresponding weights for a quarter unit circle are presented by Shivaram [24], Janssens has taken this approach and extended it to cover a full circle [4]. The integration of the TPE or TCE functional can then be performed for both the full and discontinuous part of the domain and in accordance with the stiffness difference, the total energy of the laminate can be determined.

IV. Results

In this section, the results will be presented. They consist of verification results comparing to previous work done by Kassapoglou [10] and using a isotropic plate with a cut-out as means of verification. Then a variable stiffness laminate with a linear fibre path definition is analysed.

A. Square stiffening insert

The laminate presented in Fig 1b was analysed by Kassapoglou and due to the square insert, the coordinate systems were coupled and a analytical solution was found using the energy methods and stress based approximation functions. A very similar approach to this work, and thus a good starting point to check the working of the semi-analytical model. In the work by Kassapoglou, slight differences apply with respect to the previous presented theory. First, an applied uniform force is used and thus only the first term for the potential energy is used. Second, no enriching functions are used, and the functions for N_x, N_y and N_{xy} are defined separately, while still complying to the in-plane equilibrium conditions. Using the functions and coordinate systems defined by Kassapoglou, the results presented in Fig. 4 are reproduced using the semi-analytical model. Furthermore, in Fig. 5, the axial stresses are shown in comparison to results from FEM. The plate characteristics are taken with an outer dimensions of 508×508 [mm] and three different center patch dimensions 50.8×50.8 [mm], 102×102 [mm] and 254×254 [mm]. The material properties are taken from the reference literature and consist of a plain weave fabric with $E_1 = E_2 = 67.5$ [GPa], $G_{12} = 4.48$ [GPa] and $\nu_{12} = 0.05$. The center layup consisted of layers $[(\pm 45)_5/(0/90)_2/(\pm 45)_5]$ and the perimeter layup of layers $[(\pm 45)/(0/90)_2/(\pm 45)]$.

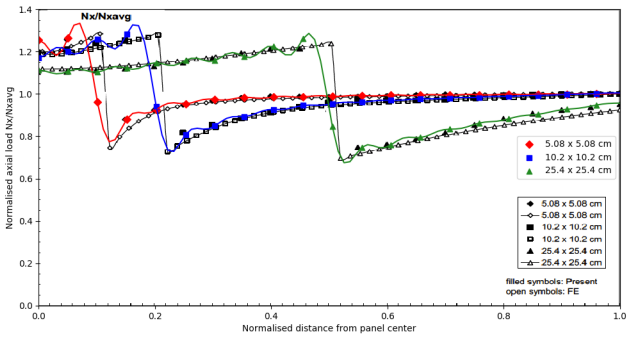

Fig. 4 Results from [10] including the recreation of the results using the semi-analytical model developed.

B. Circular stiffening insert

The next step is to check the validity of the numerical integration scheme concerning the circular integration. Also, the approximation functions as presented in this paper are used as they are deemed more suitable for circular discontinuities with respect to the functions from Kassapoglou [10], This has been checked by Janssens [4] and the approximations produce more accurate results while using less terms.

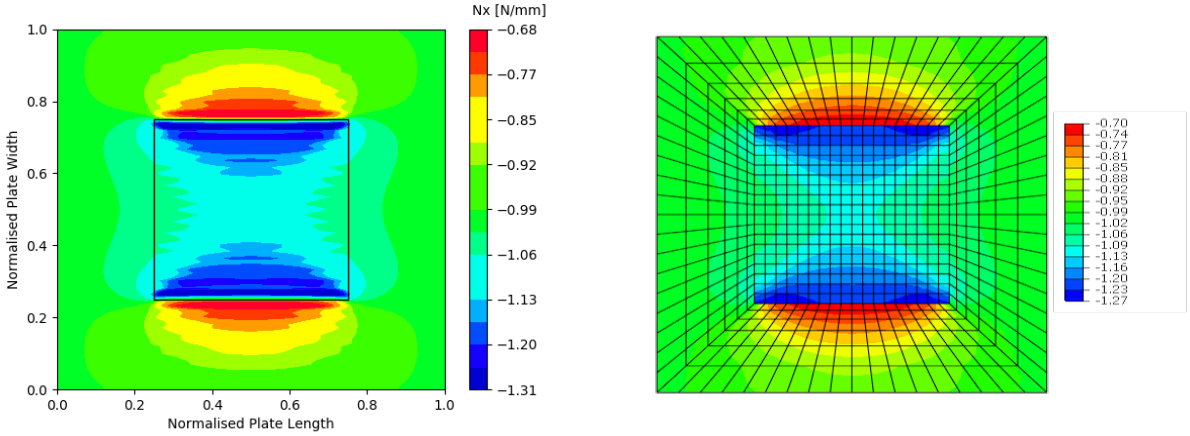

(a) Semi-analytical model **(b) ABAQUS FE**

Fig. 5 Axial loads N_x shown in comparison to those obtained from FEM.

The results for a laminate with the same materials properties and layup as the one presented in Section IV.A, loaded by uniform compressive force, containing a stiffening circular insert, are checked against results from FE software and presented in Fig. 6. Such a case could be considered where a joint is present and a hole is filled with a rivet or bolt with a higher stiffness than the sheet.

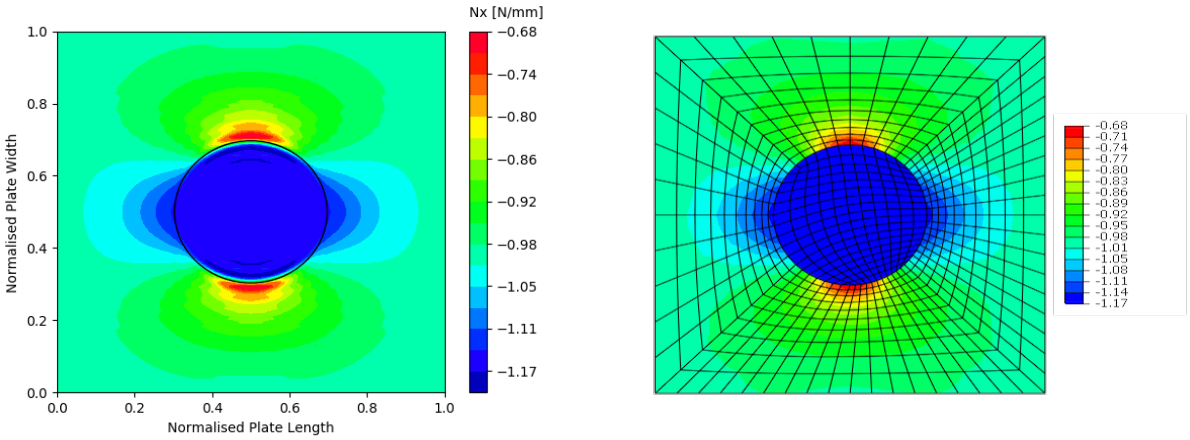

(a) Semi-analytical model **(b) ABAQUS FE**

Fig. 6 Axial loads N_x shown in comparison to those obtained from FEM.

C. Isotropic plate with a cut-out

In this section, an isotropic plate with a circular cut-out is presented. In this case the residual thickness of 2% is used as the discontinuity consists of a cut-out.

1. Pre-buckling

The material properties and plate dimensions are $E = 71$ [GPa], $\nu = 0.33$, $t = 1$ [mm], $a = b = 254$ [mm] and $R = 25$ [mm]. The plate is loaded by a uniform compressive displacement of 1 [mm]. The approximation functions include all functions described in the previous sections, Eqs. 9, 11, 12 and 13 with $I = J = K = 8$, $M = 39$ and $N = 5$ yielding a total of 524 terms, or degrees of freedom. The in-plane load distribution N_x, N_y and N_{xy} are shown in Figs. 7 and 8.

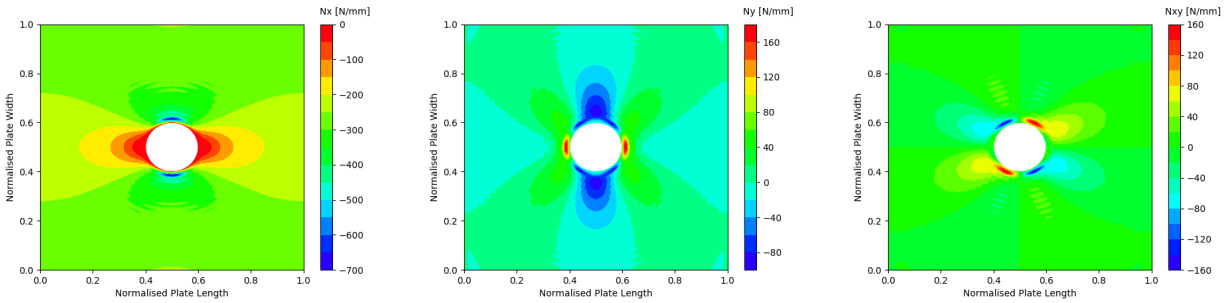

(a) N_x **(b)** N_y **(c)** N_{xy}

Fig. 7 Loads obtained from the semi-analytical model.

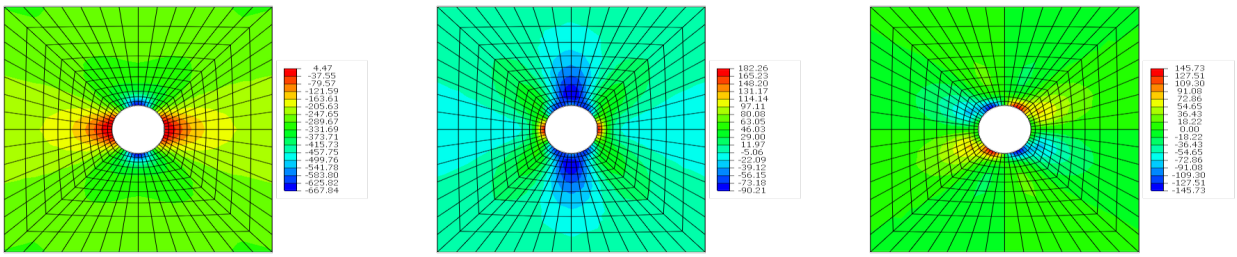

(a) N_x **(b)** N_y **(c)** N_{xy}

Fig. 8 Loads obtained from the FE model in ABAQUS.

The results show great agreement with the results from FE models. Due to the use of the residual thickness however, one observation that was made by Janssens [4], is the presence of fluctuations in the stress-field of the semi-analytical model close to the cut-out edge. This is due to the assumption made before, where the model does contain material inside the cut-out, which is made very weak as to not carry load. The semi-analytical model described this behaviour well, and so the stresses inside the cut-out area must be zero. Close to the cut-out edge in cases where there is a stress concentration, the model must make a large "jump" in stress level, whereas if the stress approaches zero near the cut-out edge, the model agrees very well. This is best illustrated when looking at the axial load N_x along two paths, at half width of the plate moving along x and at half length of the plate moving along y, as presented in Figs. 9 and 10.

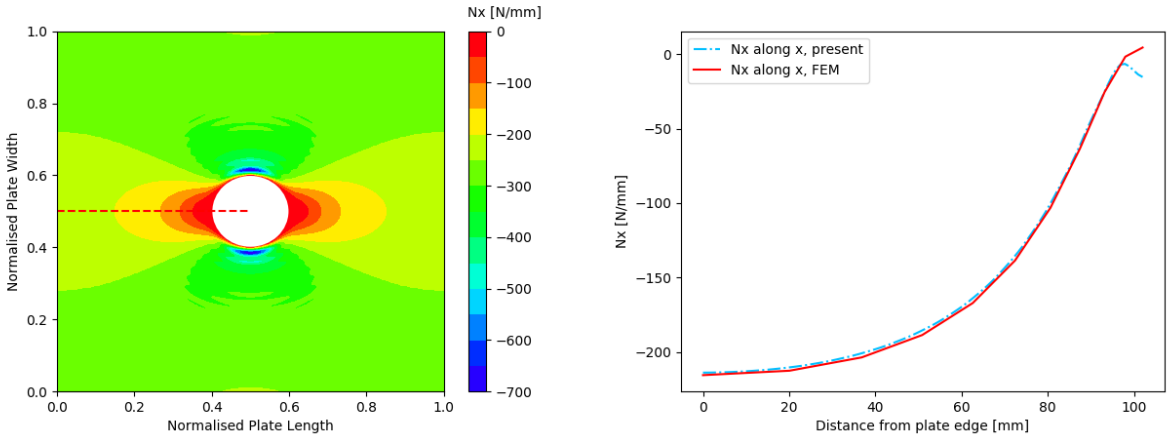

(a) Visualisation of path **(b) Axial load N_x along x**

Fig. 9 No fluctuations as loads approach zero near cut-out edge.

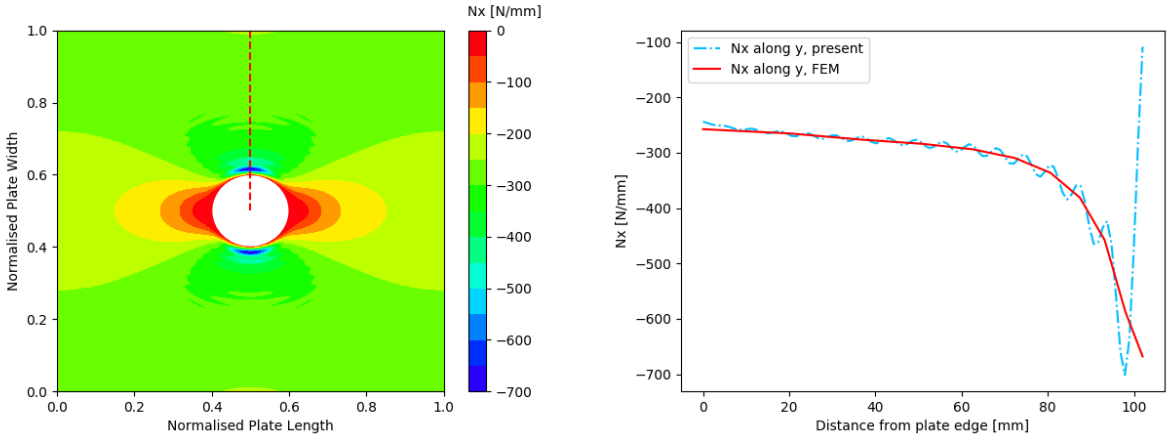

(a) Visualisation of path **(b) Axial load N_x along y**

Fig. 10 Fluctuations when loads do not approach zero near cut-out edge.

2. Buckling

With the in-plane loads determined, the buckling behaviour for the plate can be determined using the TPE and the aprroximations functions described in Eqs. 17, 18 and 19. The total number or terms taken are $I = J = 6$ and $M = N = 10$ for a total of 246 terms. The first two eigenmodes are shown in Figs. 11 and 12. The eigenvalues are presented in Table 1.

Table 1 Eigenvalues for isotropic plate containing a cut-out under uniform compressive displacement.

Mode no.	Eigenvalues		Difference [%]
	Semi-Analytical	ABAQUS	
1	0.01448	0.01427	1.47
2	0.02676	0.02630	1.75
3	0.04318	0.04302	0.37
4	0.05729	0.05742	0.23
5	0.06156	0.06098	0.95

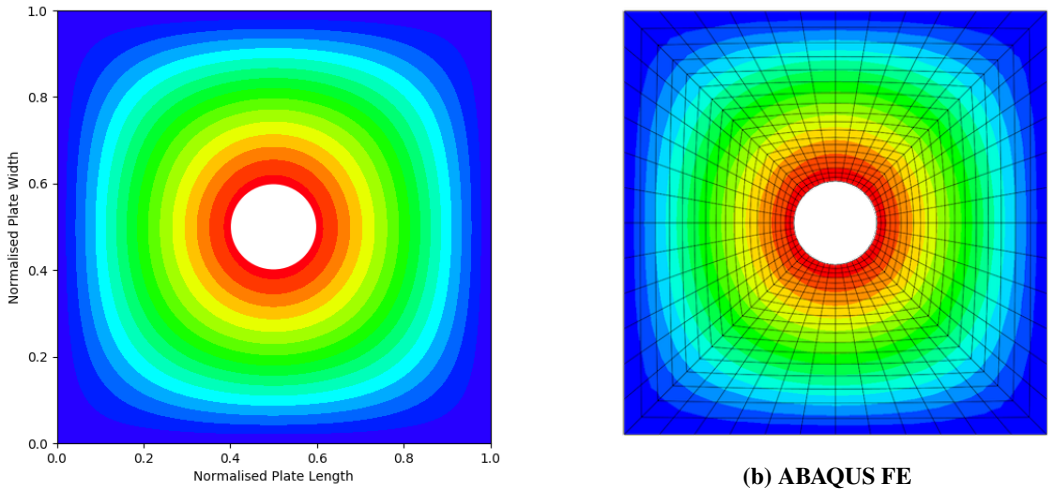

(a) Semi-analytical model **(b) ABAQUS FE**

Fig. 11 First eigenmode of isotropic plate with cut-out

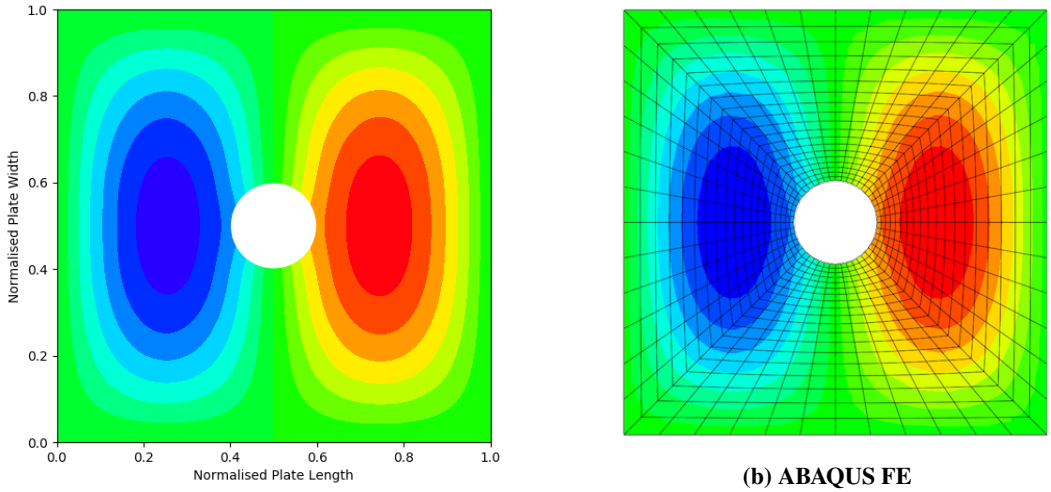

(a) Semi-analytical model **(b) ABAQUS FE**

Fig. 12 Second eigenmode of isotropic plate with cut-out

D. Variable stiffness laminate

In this section, the results for a variable stiffness laminate are presented. The laminate under consideration is defined according to the linear fibre path definition in Eq. 1 using a layup of $[90\pm < 0|75]_s$. The subsequent fibre path is shown in Fig. 13.

1. Pre-buckling

Using the TCE with Eqs. 9, 11, 12 and 13, the laminate is analysed for when loaded under a uniform compressive displacement of 1 [mm]. For the approximations functions, $I = J = K = 8$, $M = 39$ and $N = 5$. The obtained load

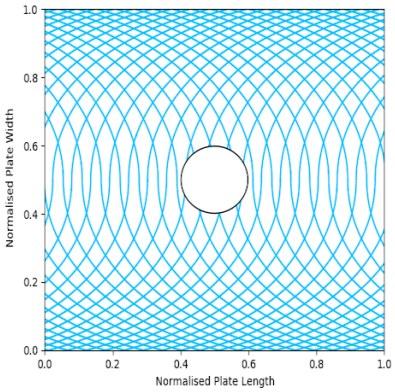

Fig. 13 Fibre path for the laminate with layup $[90\pm < 0|75]_s$ and with a circular cut-out.

distributions are shown in Figs. 14 and 15. The axial load is plotted along three different paths, the same two as in the previous section and in addition the axial loads along the width of the laminate when $x = 0$. These plots are shown in Figs. 16a through 16c. Note, that due to the variable stiffness, almost no stress concentration is present close to the cut-out edge, and thus the model shows almost no oscillations and agrees very well with the results from FE software.

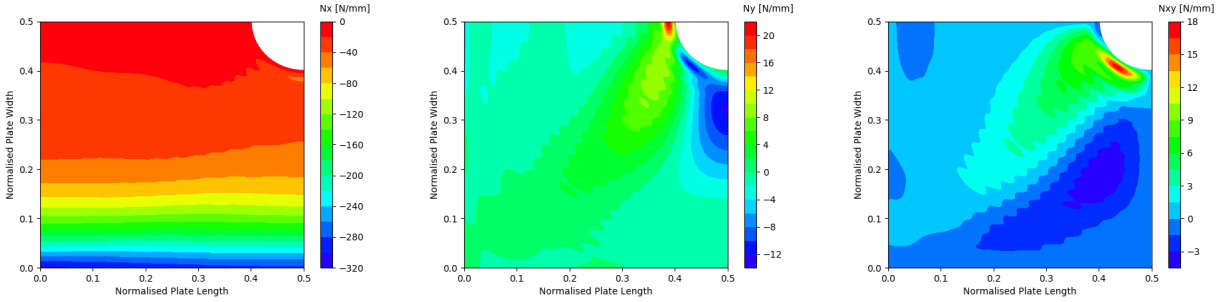

(a) N_x **(b)** N_y **(c)** N_{xy}

Fig. 14 Loads obtained from the semi-analytical model.

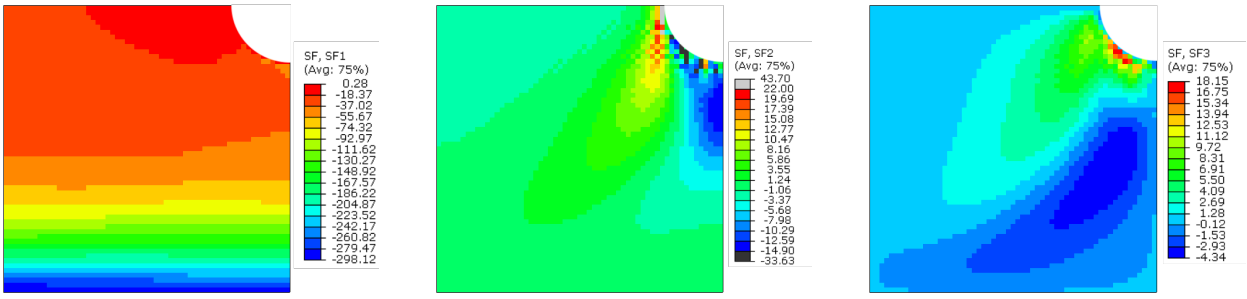

(a) N_x **(b)** N_y **(c)** N_{xy}

Fig. 15 Loads obtained from the FE software ABAQUS.

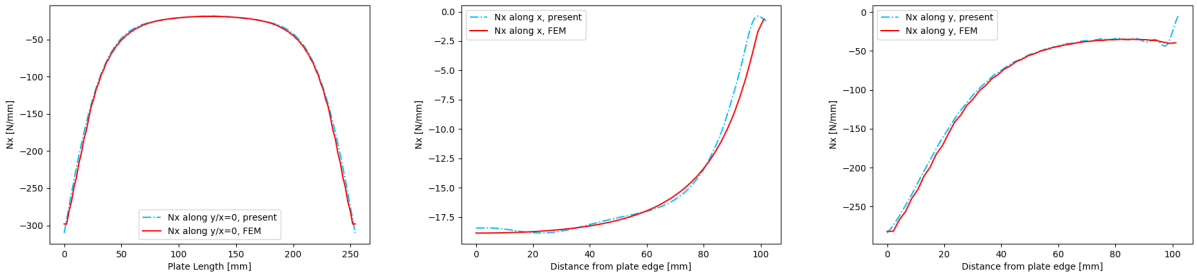

(a) Along y, $x = 0$ **(b) Along x, $y = b/2$** **(c) Along y, $x = a/2$**

Fig. 16 N_x distribution for the $[90\pm < 0|75 >]_s$ laminate, under uniform compressive displacement

2. Buckling

Using the in-plane loads, the buckling behaviour is determined and compared to the same laminate, only without a cut-out. The out-of-plane approximation functions are used with $I = J = 15$ and $M = N = 10$. The eigenvalues are shown in Table 2, and the first two eigenmodes are shown in Figs. 17 and 18. From Table 2, it can be seen that for the first eigenmode, 95% of the buckling capacity is retained while the laminate contains a cut-out.

Table 2 Eigenvalues for the VAT laminate both with and without cutout.

Mode no.	Eigenvalues	
	Pristine	Cut-Out
1	0.01262	0.01196
2	0.01300	0.01370
3	0.01790	0.01824
4	0.02441	0.02472
5	0.02668	0.02596

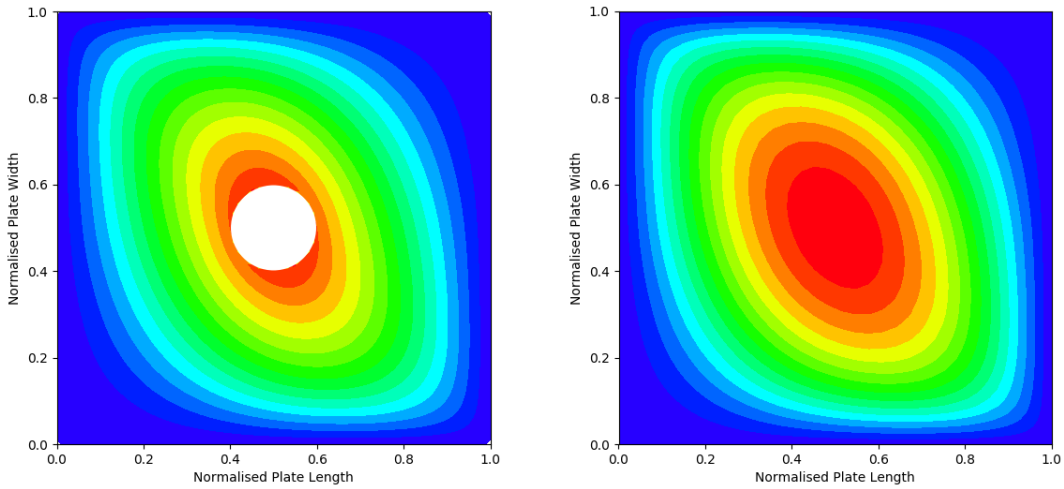

(a) With cut-out **(b) Pristine**

Fig. 17 First eigenmode for the variable stiffness laminate, with and without cut-out.

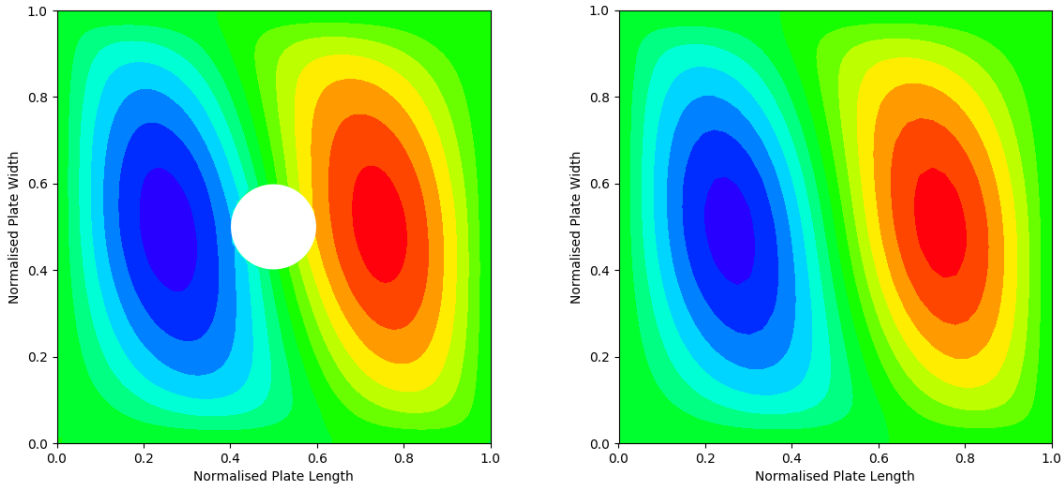

(a) With cut-out **(b) Pristine**

Fig. 18 Second eigenmode for the variable stiffness laminate, with and without cut-out.

V. Conclusions & Discussion

The semi-analytical model combined with the approximation functions presented in this work culminated in a framework capable of producing accurate results for the out-of-plane deflection, the in-plane stress distribution and the buckling behaviour of plates and laminates with discontinuities such as stiffened inserts, variable stiffness due to fibre steering and cut-outs. In the case of cut-outs, the chosen method of the Airy stress resulted in stress fluctuations near the cut-out edge. The stress-based approach was taken in order to reduce the number of unknown functions in the energy functionals, but yielded the need for additional boundary conditions on the edges of the cut-out. The main reason for this is the dependency of the different sets of trial functions on x, y, r and θ, while the boundary conditions are defined in either x and y along the outer edges or r and θ along the edge of the cut-out.

A suggested next step research would be to set up the semi-analytical model to use a displacement-based approach already for determining the in-plane stresses in the presence of discontinuities, eliminating the issues encountered at the cut-out free edge. Another improvement would be to use the non-linear strain equations to determine the in-plane and out-of-plane behaviour simultaneously via the geometric stiffness matrix [18] rather than decoupling them in the linear strain equations. The extension of the present model to a more general formulation considering non-symmetric laminates would also increase the scope of the present framework.

A. Matrix entries

The equations for the derivation of the energy matrix entries are shown here, further explanation is found in the work by Janssens [4].

A. Strain energy, U

$$\begin{bmatrix} \mathbf{K} & \mathbf{K_C} \\ \mathbf{K_C}^T & \mathbf{C} \end{bmatrix} \begin{Bmatrix} \boldsymbol{\varphi} \\ \mathbf{c} \end{Bmatrix} = \begin{Bmatrix} \mathbf{0} \\ \mathbf{Px0} \end{Bmatrix}$$

$$U = \frac{1}{2} \iint_{\Omega} \left(a_{11} N_x^2 + a_{22} N_y^2 + 2 a_{12} N_x N_y + a_{66} N_{xy}^2 \right) d\Omega \tag{21}$$

$$U = \frac{1}{2}\iint_{\Omega}\Big\{a_{11}\left(\Phi_{0,yy}+\Phi_{1,yy}+\Phi_{2,yy}+\Phi_{3,yy}\right)^2 + a_{22}\left(\Phi_{0,xx}+\Phi_{1,xx}+\Phi_{2,xx}+\Phi_{3,xx}\right)^2 + a_{12}\left(\Phi_{0,yy}+\Phi_{1,yy}+\Phi_{2,yy}+\Phi_{3,yy}\right)\left(\Phi_{0,xx}+\Phi_{1,xx}+\Phi_{2,xx}+\Phi_{3,xx}\right) + a_{66}\left(-\Phi_{0,xy}-\Phi_{1,xy}-\Phi_{2,xy}-\Phi_{3,xy}\right)^2\Big\}\,d\Omega$$

As Φ_0 is the edge load function, it only has a value for N_x, so $\Phi_{0,xx} = \Phi_{0,xy} = 0$. Expanding the equation further yields:

$$\begin{aligned}U = \frac{1}{2}\iint_{\Omega}\Big\{a_{11}\Big(&\Phi_{0,yy}^2+\Phi_{1,yy}^2+\Phi_{2,yy}^2+\Phi_{3,yy}^2+2\Phi_{0,yy}\Phi_{1,yy}\\ &+2\Phi_{0,yy}\Phi_{2,yy}+2\Phi_{0,yy}\Phi_{3,yy}+2\Phi_{1,yy}\Phi_{2,yy}+2\Phi_{1,yy}\Phi_{3,yy}+2\Phi_{2,yy}\Phi_{3,yy}\Big)\\ &+a_{22}\Big(\Phi_{1,xx}^2+\Phi_{2,xx}^2+\Phi_{3,xx}^2+2\Phi_{1,xx}\Phi_{2,xx}+2\Phi_{1,xx}\Phi_{3,xx}+2\Phi_{2,xx}\Phi_{3,xx}\Big)\\ &+2a_{12}\left(\Phi_{0,yy}\Phi_{1,xx}+\Phi_{0,yy}\Phi_{2,xx}+\Phi_{0,yy}\Phi_{3,xx}+\Phi_{1,yy}\Phi_{1,xx}+\Phi_{1,yy}\Phi_{2,xx}+\Phi_{1,yy}\Phi_{3,xx}\right.\\ &\left.+\Phi_{2,yy}\Phi_{1,xx}+\Phi_{2,yy}\Phi_{2,xx}+\Phi_{2,yy}\Phi_{3,xx}+\Phi_{3,yy}\Phi_{1,xx}+\Phi_{3,yy}\Phi_{2,xx}+\Phi_{3,yy}\Phi_{3,xx}\right)\\ &+a_{66}\Big(\Phi_{1,xy}^2+\Phi_{2,xy}^2+\Phi_{3,xy}^2+2\Phi_{1,xy}\Phi_{2,xy}+2\Phi_{1,xy}\Phi_{3,xy}+2\Phi_{2,xy}\Phi_{3,xy}\Big)\Big\}\,d\Omega\end{aligned}$$

Collecting terms which correspond to the coupling between the various sets of trial functions will then give the energy expressions which will lead to the corresponding matrix entry.

$$\begin{aligned}U_{00} &= \frac{1}{2}\iint_{\Omega}\left(a_{11}\Phi_{0,yy}^2\right)d\Omega\\ U_{11} &= \frac{1}{2}\iint_{\Omega}\left(a_{11}\Phi_{1,yy}^2+a_{22}\Phi_{1,xx}^2+a_{66}\Phi_{1,xy}^2+2a_{12}\Phi_{1,yy}\Phi_{1,xx}\right)d\Omega\\ U_{22} &= \frac{1}{2}\iint_{\Omega}\left(a_{11}\Phi_{2,yy}^2+a_{22}\Phi_{2,xx}^2+a_{66}\Phi_{2,xy}^2+2a_{12}\Phi_{2,yy}\Phi_{2,xx}\right)d\Omega\\ U_{33} &= \frac{1}{2}\iint_{\Omega}\left(a_{11}\Phi_{3,yy}^2+a_{22}\Phi_{3,xx}^2+a_{66}\Phi_{3,xy}^2+2a_{12}\Phi_{3,yy}\Phi_{3,xx}\right)d\Omega\\ U_{01} &= \iint_{\Omega}\left(a_{11}\Phi_{0,yy}\Phi_{1,yy}+a_{12}\Phi_{0,yy}\Phi_{1,xx}\right)d\Omega\\ U_{02} &= \iint_{\Omega}\left(a_{11}\Phi_{0,yy}\Phi_{2,yy}+a_{12}\Phi_{0,yy}\Phi_{2,xx}\right)d\Omega\\ U_{03} &= \iint_{\Omega}\left(a_{11}\Phi_{0,yy}\Phi_{3,yy}+a_{12}\Phi_{0,yy}\Phi_{3,xx}\right)d\Omega\\ U_{12} &= \iint_{\Omega}\left(a_{11}\Phi_{1,yy}\Phi_{2,yy}+a_{22}\Phi_{1,xx}\Phi_{2,xx}+a_{66}\Phi_{1,xy}\Phi_{2,xy}+a_{12}\left[\Phi_{1,yy}\Phi_{2,xx}+\Phi_{1,xx}\Phi_{2,yy}\right]\right)d\Omega\\ U_{13} &= \iint_{\Omega}\left(a_{11}\Phi_{1,yy}\Phi_{3,yy}+a_{22}\Phi_{1,xx}\Phi_{3,xx}+a_{66}\Phi_{1,xy}\Phi_{3,xy}+a_{12}\left[\Phi_{1,yy}\Phi_{3,xx}+\Phi_{1,xx}\Phi_{3,yy}\right]\right)d\Omega\\ U_{23} &= \iint_{\Omega}\left(a_{11}\Phi_{2,yy}\Phi_{3,yy}+a_{22}\Phi_{2,xx}\Phi_{3,xx}+a_{66}\Phi_{2,xy}\Phi_{3,xy}+a_{12}\left[\Phi_{2,yy}\Phi_{3,xx}+\Phi_{2,xx}\Phi_{3,yy}\right]\right)d\Omega\end{aligned}$$

The entries for the matrices $\mathbf{K}, \mathbf{Kc}$ and $\mathbf{C}$ are obtained by minimising the energy expressions above with their respective unknown coefficient.

$$[\mathbf{K}]\,\{\varphi\} = \begin{bmatrix} \frac{\partial U_{11}}{\partial A_{ij}} & \frac{\partial U_{12}}{\partial A_{ij}} & \frac{\partial U_{13}}{\partial A_{ij}} \\ \frac{\partial U_{12}}{\partial B_{mn}} & \frac{\partial U_{22}}{\partial B_{mn}} & \frac{\partial U_{23}}{\partial B_{mn}} \\ \frac{\partial U_{13}}{\partial C_{mn}} & \frac{\partial U_{23}}{\partial C_{mn}} & \frac{\partial U_{33}}{\partial C_{mn}} \end{bmatrix}$$

$$[\mathbf{Kc}]\,\{\mathbf{c}\} = \begin{Bmatrix} \frac{\partial U_{01}}{\partial A_{ij}} \\ \frac{\partial U_{02}}{\partial B_{mn}} \\ \frac{\partial U_{03}}{\partial C_{mn}} \end{Bmatrix}$$

$$[\mathbf{C}]\,\{\mathbf{c}\} = \begin{bmatrix} \frac{\partial U_{00}}{\partial c_k} \end{bmatrix}$$

B. Potential energy, V

$$V = -\int_0^b \left[\Phi_{,yy} u\right]_{x=0}^{x=a} dy \tag{22}$$

$$V = -\int_0^b \left[u\left(\Phi_{0,yy} + \Phi_{1,yy} + \Phi_{2,yy} + \Phi_{3,yy}\right)\right]_{x=0}^{x=a} dy$$

$$V = -\int_0^b \Delta_x \Phi_{0,yy}\, dy$$

$$V = -\Delta_x \int_0^b \Phi_{0,yy}\, dy$$

$$V = -\Delta_x \int_0^b \sum_{k=0}^{K} c_k \cdot L_k(y)\, dy$$

$$\mathbf{Px0} = -\Delta_x \begin{bmatrix} b \\ 0 \\ \vdots \\ 0 \end{bmatrix} \begin{matrix} (k{=}0) \\ (k{=}1) \\ \vdots \\ (k{=}K) \end{matrix}$$

References

[1] Gürdal, Z., and Olmedo, R., "In-plane response of laminates with spatially varying fiber orientations - Variable stiffness concept," *AIAA Journal*, Vol. 31, No. 4, April, 1993, pp. 751–758. https://doi.org/10.2514/3.11613.

[2] Alhajahmad, A., Abdalla, M. M., and Gürdal, Z., "Design Tailoring for Pressure Pillowing Using Tow-Placed Steered Fibers," Ph.D. thesis, 2008. https://doi.org/10.2514/1.32676.

[3] Wu, Z., Weaver, P. M., Raju, G., Kim, B. C., and Chul Kim, B., "Buckling analysis and optimisation of variable angle tow composite plates," *Thin-Walled Structures*, 2012. https://doi.org/10.1016/j.tws.2012.07.008.

[4] Janssens, T. A., "Semi-Analytical Modelling of VAT Laminates with Cut-Outs: Behaviour of Discontinuous Variable Stiffness Laminates Using Enriched Rayleigh-Ritz Method," MSc Thesis, Delft University of Technology, 2020. URL http://resolver.tudelft.nl/uuid:ee695858-bcee-4118-8181-d0c3729b7ef1.

[5] Huang, C. S., Leissa, A. W., and Li, R. S., "Accurate vibration analysis of thick, cracked rectangular plates," *Journal of Sound and Vibration*, Vol. 330, No. 9, 2011, pp. 2079–2093.

[6] Milazzo, A., Benedetti, I., and Gulizzi, V., "An extended Ritz formulation for buckling and post-buckling analysis of cracked multilayered plates," *Composite Structures*, Vol. 201, No. June, 2018, pp. 980–994. https://doi.org/10.1016/j.compstruct.2018.06.026.

[7] Castro, S. G., Donadon, M. V., and Guimarães, T. A., "ES-PIM applied to buckling of variable angle tow laminates," *Composite Structures*, Vol. 209, 2019, pp. 67–78. https://doi.org/10.1016/j.compstruct.2018.10.058, URL https://linkinghub.elsevier.com/retrieve/pii/S0263822318322979.

[8] Wang, Z., Almeida Jr., J. H. S., St-Pierre, L., Wang, Z., and Castro, S. G., "Reliability-based buckling optimization with an accelerated Kriging metamodel for filament-wound variable angle tow composite cylinders," *Composite Structures*, Vol. 254, 2020, p. 112821. https://doi.org/10.1016/j.compstruct.2020.112821, URL https://linkinghub.elsevier.com/retrieve/pii/S0263822320327471.

[9] Biggers, S. B., and Srinivasan, S., "Compression Buckling Response of Tailored Rectangular Composite Plates," *AIAA Journal*, 1993. https://doi.org/10.2514/3.61543.

[10] Kassapoglou, C., "Composite plates with two concentric layups under compression," *Composites Part A: Applied Science and Manufacturing*, Vol. 39, No. 1, 2008, pp. 104–112. https://doi.org/10.1016/j.compositesa.2007.08.024.

[11] Guimaraes, T. A., Castro, S. G., Rade, D. A., and Cesnik, C. E., "Panel Flutter Analysis and Optimization of Composite Tow Steered Plates," *58th AIAA/ASCE/AHS/ASC Structures, Structural Dynamics, and Materials Conference*, , No. January, 2017.

[12] Castro, S. G., and Donadon, M. V., "Assembly of semi-analytical models to address linear buckling and vibration of stiffened composite panels with debonding defect," *Composite Structures*, Vol. 160, 2017, pp. 232–247. https://doi.org/10.1016/j.compstruct.2016.10.026, URL http://linkinghub.elsevier.com/retrieve/pii/S026382231631008Xhttps://linkinghub.elsevier.com/retrieve/pii/S026382231631008X.

[13] de Matos Junior, O. D., Donadon, M. V., and Castro, S. G., "Aeroelastic behavior of stiffened composite laminated panel with embedded SMA wire using the hierarchical Rayleigh–Ritz method," *Composite Structures*, Vol. 181, 2017, pp. 26–45. https://doi.org/10.1016/j.compstruct.2017.08.060, URL http://www.scopus.com/inward/record.url?eid=2-s2.0-85028415617&partnerID=MN8TOARShttps://linkinghub.elsevier.com/retrieve/pii/S0263822317311807.

[14] Vescovini, R., Dozio, L., D'Ottavio, M., and Polit, O., "On the application of the Ritz method to free vibration and buckling analysis of highly anisotropic plates," *Composite Structures*, Vol. 192, 2018, pp. 460–474. https://doi.org/10.1016/j.compstruct.2018.03.017, URL https://www.sciencedirect.com/science/article/pii/S0263822318305233#f0030https://linkinghub.elsevier.com/retrieve/pii/S0263822318305233.

[15] Bardell, N., "Free vibration analysis of a flat plate using the hierarchical finite element method," *Journal of Sound and Vibration*, Vol. 151, No. 2, 1991, pp. 263–289. https://doi.org/10.1016/0022-460X(91)90855-E, URL https://linkinghub.elsevier.com/retrieve/pii/0022460X9190855E.

[16] Bardell, N. S., Dunsdon, J. M., and Langley, R. S., "On the free vibration of complelety free, open , cylindrically curved isotropic shell panels," *Journal of Sound and Vibration*, Vol. 207, No. 5, 1997, pp. 647–669. https://doi.org/10.1006/jsvi.1997.1115, URL http://linkinghub.elsevier.com/retrieve/pii/S0022460X97911159.

[17] Vescovini, R., and Bisagni, C., "Buckling analysis and optimization of stiffened composite flat and curved panels," *AIAA Journal*, Vol. 50, No. 4, 2012, pp. 904–915. https://doi.org/10.2514/1.J051356, URL https://arc.aiaa.org/doi/abs/10.2514/1.J051356.

[18] Castro, S. G. P., Mittelstedt, C., Monteiro, F. A. C., Arbelo, M. A., Ziegmann, G., and Degenhardt, R., "Linear buckling predictions of unstiffened laminated composite cylinders and cones under various loading and boundary conditions using semi-analytical models," *Composite Structures*, Vol. 118, No. 1, 2014, pp. 303–315. https://doi.org/10.1016/j.compstruct.2014.07.037, URL http://www.scopus.com/inward/record.url?eid=2-s2.0-84919711488&partnerID=MN8TOARShttps://linkinghub.elsevier.com/retrieve/pii/S0263822314003602http://dx.doi.org/10.1016/j.compstruct.2014.07.037.

[19] Castro, S. G. P., Guimarães, T. A. M., Rade, D. A., and Donadon, M. V., "Flutter of stiffened composite panels considering the stiffener's base as a structural element," *Composite Structures*, Vol. 140, 2016, pp. 36–43. https://doi.org/10.1016/j.compstruct.2015.12.056, URL https://doi.org/10.1016/j.compstruct.2015.12.056https://linkinghub.elsevier.com/retrieve/pii/S0263822315011460http://www.scopus.com/inward/record.url?eid=2-s2.0-84953212729&partnerID=MN8TOARS.

[20] Som, P., and Deb, A., "A generalized Ritz-based method for nonlinear buckling of thin cylindrical shells," *Thin-Walled Structures*, Vol. 76, 2014, pp. 14–27. https://doi.org/10.1016/j.tws.2013.09.024.

[21] Milazzo, A., and Oliveri, V., "Post-buckling analysis of cracked multilayered composite plates by pb-2 Rayleigh-Ritz method," *Composite Structures*, Vol. 132, 2015, pp. 75–86. https://doi.org/10.1016/j.compstruct.2015.05.007.

[22] Castro, S. G. P., Mittelstedt, C., Monteiro, F. A. C., Arbelo, M. A., Degenhardt, R., and Ziegmann, G., "A semi-analytical approach for linear and non-linear analysis of unstiffened laminated composite cylinders and cones under axial, torsion and pressure loads," *Thin-Walled Structures*, Vol. 90, 2015, pp. 61–73. https://doi.org/10.1016/j.tws.2015.01.002, URL http://www.scopus.com/inward/record.url?eid=2-s2.0-84921957823&partnerID=MN8TOARShttps://linkinghub.elsevier.com/retrieve/pii/S0263823115000051.

[23] Castro, S. G. P., Mittelstedt, C., Monteiro, F. A. C., Degenhardt, R., and Ziegmann, G., "Evaluation of non-linear buckling loads of geometrically imperfect composite cylinders and cones with the Ritz method," *Composite Structures*, Vol. 122, 2015, pp. 284–299. https://doi.org/10.1016/j.compstruct.2014.11.050, URL http://dx.doi.org/10.1016/j.compstruct.2014.11.050http://www.scopus.com/inward/record.url?eid=2-s2.0-84919770071&partnerID=MN8TOARShttps://linkinghub.elsevier.com/retrieve/pii/S026382231400631X.

[24] Shivaram, K. T., "Gauss Legendre quadrature over a unit circle," *International Journal of Engineering and Technical Research*, Vol. 2, No. 9, September, 2013.